JOURNAL OF CATALYSIS **159,** 332–339 (1996)
ARTICLE NO. 0095

Characterization of the Structure and Catalytic Behavior of $AlF_{3-x}(OH)_x$ with Aluminum Successively Replaced by Chromium and Magnesium

E. Kemnitz,[1] A. Hess, G. Rother, and S. Troyanov

[*] *Institut für Chemie der Humboldt-Universität zu Berlin, Hessische Str. 1/2, D-10115 Berlin, Germany*

Received February 27, 1995; revised October 26, 1995; accepted November 30, 1995

The calcination of α-$AlF_3 \cdot 3H_2O$ forms a β-AlF_3 phase which is catalytically active for dismutation of C_1-hydrocarbons such as dichlorodifluoromethane. The stepwise replacement of aluminum by chromium and magnesium leads to considerable alterations in structure and surface properties of the calcination products. This is accompanied by significant changes in the catalytic activity. The synthesis of the catalysts was carried out by coprecipitation of mixed metal fluoride trihydrates and subsequent calcination procedures. The stepwise replacement with chromium leads to a rebuilding of the lattice from the pseudo-hexagonal tungsten bronze (HTB) structure of β-AlF_3 into a cubic pyrochlore structure of $CrF_{3-x}(OH)_x$. Hexagonal β-CrF_3 or mixed crystals β-$(Al,Cr)F_3$ were not obtained via this route. The maximum catalytic activity for CCl_2F_2 dismutation was obtained for the 50% chromium sample, which is accompanied by a maximum BET surface area and a maximum number of Lewis acid sites. $CrF_{3-x}(OH)_x$ exhibits a dramatic loss of catalytic activity as well as BET surface area. Possible explanations are given by comparing the pseudo-hexagonal tungsten bronze structure with the cubic pyrochlore structure with regard to accessibility of the Lewis acid metal cations. The presence of hydroxyl groups within the pyrochlore lattice enables the formation of hydrogen bridge bonds which is accompanied by a shielding of the metal cations. In the case of the replacement with magnesium the aim was to tune the strength of the Lewis acidity. The catalytic activity of the calcined samples passes through a maximum at the 10% magnesium sample. Due to the decrease of the strength of Lewis acid sites with further increasing Mg content, the catalytic activity is more and more diminished. At 50% Mg and higher the strength of the Lewis acid sites is no longer sufficient to catalyze the dismutation. © 1996 Academic Press, Inc.

INTRODUCTION

Fluorinated aluminum oxides and aluminum fluorides are widely used as catalysts for the heterogeneous Cl/F exchange on hydrochlorocarbons. It is well established that the addition of further metal ions affects the activity and stability of the catalyst. The most common catalyst preparation method is based on the impregnation of γ-alumina with metal salt solutions and subsequent HF treatment. For the manufacture of CF_3–CH_2F by fluorination of CF_3–CH_2Cl with HF the catalyst consists of a metal fluoride (e.g., Co, La, Ni, Mg, or Ru) supported on AlF_3. It is obtained by fluorination of impregnated Al_2O_3 using HF (1). A very similar procedure is reported for a chromium-doped alumina (2). Further doping metals are Fe and Mn (3), leading to a minimization of undesired side products.

Unfortunately, there are invariably insufficient data in patents about the crystal modification and surface properties of the fluorinated catalysts. The pure oxides are not active. A preactivation with hydrogen fluoride or fluorine-containing halocarbons is required. After that, the surfaces contain metastable metal fluoride species, e.g., β-aluminum fluoride (4). Dismutation reactions are observed during and after activation with C_1 halocarbons such as $CHClF_2$ or CCl_2F_2. The reaction pathway proceeds via preadsorption of the C_1 haloalkane on strong Lewis acid sites (5).

For a better understanding of the activity or inactivity of solid phases it is desirable to simplify the complex situation on the surface of fluorinated oxides. Therefore, it is useful to investigate those metal fluoride phases which can be identified after activation processes. Here, β-aluminum fluoride plays the most important role (4, 5). It is a good model substance for the investigation of metal doping influence on Lewis acidity and catalytic activity. In the literature about replacement and doping effects on the catalytic activity there are many publications about the γ-alumina system, but almost nothing about cationic replacement on aluminum fluoride. Nevertheless, some experiences might be transferred from the γ-oxide into the β-fluoride system.

γ-alumina has been doped with alkaline metals (6, 7), alkaline earth metals (8), transition elements (9, 10), rare earth metals (11), and elements of the fourth main group (12). A replacement of Al with Mg in γ-alumina results in a decrease of acid sites of weak and medium strength, whereas the strong sites remain unchanged (6). Since the dehydration of the probe molecule 1-butanol was found to

[1] To whom correspondence should be addressed.

0021-9517/96 $18.00

decrease with increasing Mg content, it was concluded that Lewis acid sites of medium strength are responsible for the catalysis of the probe reaction. The diminishing of acidity is accompanied by an increase of basicity (7, 13).

Many authors have studied the Brønsted acidity as a function of the dopant concentration (e.g., Ref. (9) and references therein), but here it is obvious that any prediction of behavior cannot be transferred to the metal fluoride system since Brønsted acidity is not expected on the surface of pure fluorides. In contrast, fluorinated oxides as well as partially hydrolyzed metal halides exhibit Brønsted acidity (5, 14).

There are in fact two reasons to investigate the influence of metal replacement on the catalytic activity in the β-AlF_3 system:

(i) There is no evidence, yet as to where the doping metals on fluorinated oxide surfaces are located. Two cases are possible; either they statistically replace aluminum, or there are several solid phases in the surface region. In fact, there are only a few publications that deal with the characterization of the surface phases formed during the activation procedure (e.g., (4, 5, 14, 15)).

(ii) Even if one starts from well-defined doped oxide phases, it is not expected that one will obtain well defined fluorinated phases after activation.

For these reasons this paper deals with cationic replacement on α-$AlF_3 \cdot 3H_2O$ (which is the precursor of β-AlF_3) to enable comparisons to be made between catalytic effects and doping-induced alterations in structure and surface properties.

As replacing metals those were selected which are reported to have catalytic effects, e.g., chromium ($r_{Cr^{3+}} = 62$pm) or magnesium $r_{Mg^{2+}} = 72$ pm) (compare $r_{Al^{3+}} = 54$ pm (16)). All modified catalysts were prepared by coprecipitation of metal fluoride trihydrates (Al, Cr) or metal fluorides (Mg) and subsequent calcination. Depending on the amount of Cr and Mg the calcination products offered different degrees of partial hydrolysis, different lattices, different surface acidities, and, therefore, different catalytic properties. The alterations are presented as a function of the dopant concentration (varying from 0 mol% up to 100 mol% content of the replacing metal ion). Interactions between surface, structure, and Lewis acidity are discussed.

EXPERIMENTAL

Preparation of the Catalysts

Basic aluminum acetate $Al(OH)(CH_3COO)_2$ was dissolved in 40 wt% hydrofluoric acid. A solution of the doping agent was prepared by dissolving chromium(III) nitrate or magnesium nitrate in ethanol, respectively. Then, the latter solution was added to the first. The precipitate was separated and calcined under argon flow (temperature program, maximum 420°C). The sample powder was covered by aluminum foil to allow a "self-produced atmosphere." The concentration of the replacing metal is given in mol% of the total metal content. All sample notations refer to the concentrations of the initial solutions. The final metal contents (calcined precipitates) were determined by ICP-AES for those samples that were soluble in phosphoric acid (standard deviation ±1%).

All samples were characterized by X-ray powder diffraction (Cu$K\alpha$ radiation) and FTIR photoacoustic spectroscopy. The determination of the fluoride contents was carried out according to Ref. (17). The standard deviation was below 2%. The specific surface areas of the samples were determined using a ASAP 2000 system (Micromeritics) based on the nitrogen BET method (maximum experimental error ±1%).

Determination of Catalytic Activity

The probe reaction used is the dismutation of CCl_2F_2,

$$2CCl_2F_2 \rightleftarrows CClF_3 + CCl_3F. \qquad [1]$$

The products undergo further dismutation reactions (18, 19). In detail, a constant weight of 0.6 g of the catalyst was used in a flow reactor (nickel tube). A residence time of 2 s was set up by adjusting the appropriate gas flow. First, the sample was calcined under nitrogen flow at 400°C for 1 h and then subsequently treated with a CCl_2F_2 flow at 390°C. The composition of the gas phase at the exit of the reactor was determined by gas chromatography column: Poraplot u, i.d. 0.53 mm, length 25 m). Results will be presented as plots of the conversion of the starting substance CCl_2F_2 due to the dismutation reaction in Eq. [1] versus time of activation. The experimental error on the conversion did not exceed ±5%.

Temperature-Programmed Desorption

The temperature-programmed desorption of ammonia as probe molecule was employed for the determination of the strength distribution of acid sites. An adsorption feed of 18 ml ammonia was fed to 0.5 g of the solid sample at 100°C (flow system, permanent nitrogen flow). After that, a temperature program was started (following the feed pulse for 5 min isothermally 100°C, programming at 7.5 K/min up to 475°C, total run time 55 min). An FTIR flow cell was used for detection of desorbed ammonia. Further details are given in Ref. (5). Tables 1 and 2 present amounts of desorbed ammonia per gram of catalyst with regard to the relevant desorption temperature region between 325–400°C. Previous studies (5) have shown that this particular acid strength interval correlates with the catalytic activity.

TABLE 1

Element Composition, Specific Surface Area (BET), and Amount of Desorbed Ammonia (TPD region 325–400°C) of Various Cr Replaced α-$AlF_3 \cdot 3H_2O$ Calcination Products

Cr/(Cr + Al) (precursors) (mol%)	Atomic composition[a] (final products, molar ratio) Al : Cr : F : O : H	Specific surface area (m^2/g)	Desorbed ammonia (mmol/g)
0	[b]	31	220
3	[b]	43	213
10	0.9 : 0.1 : 3	54	237
50	0.66 : 0.34 : 2.0 : 0.5	121	343
80	0.42 : 0.58 : 1.5 : 1.5 : 1.5	100	161
100	1 : 0.94 : 2.06 : 2.06	5	101

[a] Determined by ICP-AES.
[b] Not determined, sample insoluble.

Infrared Photoacoustic Spectroscopy of Chemisorbed Pyridine

This method was employed for the determination of the nature of acid sites (Lewis and/or Brønsted) on the catalyst surfaces. 30 μl of liquid pyridine was injected into a vaporizer (located on the inlet of the reactor, permanent nitrogen flow) and passed to 70 mg of the solid sample at 150°C in a flow system. The excess gaseous and physisorbed pyridine was removed by purging with dried nitrogen. After cooling to room temperature the sample was transferred into a MTECH photoacoustic cell coupled with a FTIR spectrometer. The whole procedure was carried out under the same conditions as described previously (5).

RESULTS

Replacement by Chromium

The precipitates that were obtained after mixing the two components (see Experimental section) consisted of α-$AlF_3 \cdot 3H_2O$/ α-$CrF_3 \cdot 3H_2O$ mixtures. There was no evidence for the formation of mixed crystals (solid solutions) with mutual replacement in the lattices. After the calcination the following XRD results were obtained (compare Fig. 1). At and below 10% Cr the reflections of the pseudo-hexagonal tungsten bronze (HTB) structure of β-AlF_3 (20, 4) have been detected, whereas the intensities diminish with increasing Cr content. An alteration of the lattice constants was not observed. This indicates that chromium is not incorporated into the β-AlF_3 lattice.

The 50 and 80% Cr samples appeared to be substantially amorphous, whereas a new phase became visible on increasing the Cr content further (Fig. 1). This new phase is the dehydrated cubic pyrochlore structure of

TABLE 2

Element Composition, Specific Surface Area (BET) and Amount of Desorbed Ammonia (TPD Region 325–400°C) of Various Mg-replaced α-$AlF_3 \cdot 3H_2O$ Calcination Products

Mg/(Mg + Al) (precursors) (mol%)	Atomic composition (final products, molar ratio) Al : Mg : F : O : H	Specific surface area (m^2/g)	Desorbed ammonia (mmol/g)
0	[b]	31	222
3	[b]	33	230
10	[b]	40	242
50	0.45 : 0.55 : 1.85 : 0.3	45	135
100	1 : 2	57	137

[a] Determined by ICP-AES.
[b] Not determined, sample insoluble.

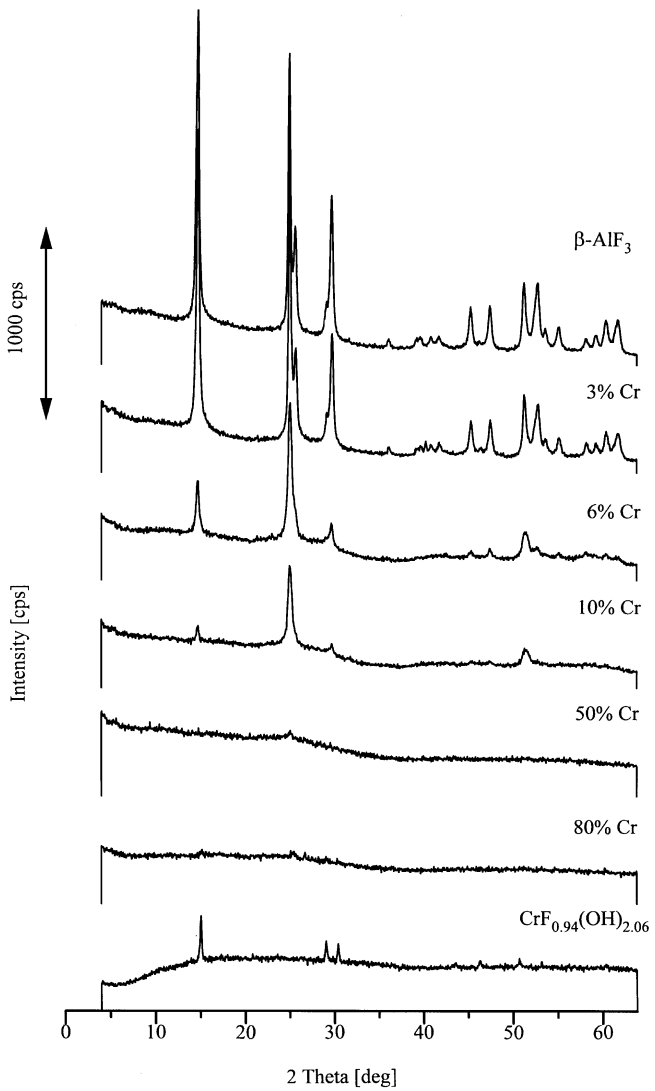

FIG. 1. XRD patterns (offset) of α-$AlF_3 \cdot 3H_2O$ calcination products with stepwise replacement by Cr. Note the change from the β-AlF_3 structure into the pyrochlore structure of $CrF_{3-x}(OH)_x$ with increasing Cr content.

$CrF_{3-x}(OH)_x \cdot yH_2O$ (21). Table 1 gives a survey of the sample compositions, specific surface areas, and amounts of ammonia desorption. It is remarkable that under identical conditions (starting substances α-$AlF_3 \cdot 3H_2O$ and α-$CrF_3 \cdot 3H_2O$) using the Al compound β-AlF_3 is obtained, whereas in the Cr system a partial hydrolysis forming, e.g., $CrF_{0.94}(OH)_{2.06}$ occurs. β-CrF_3 (20), which is isotypic with β-AlF_3, and $AlF_{3-x}(OH)_x$, (22, 23), which is isotypic with the corresponding Cr compound, were not observed.

Higher calcination temperatures were not practicable, since the catalytically inactive, stable α-metal fluorides would have been formed by crystallographic phase transition (5). In the case of the chromium hydroxyfluoride, the hydrolysis would continue at higher temperatures leading to an immediate formation of α-Cr_2O_3 at approximately 500°C. As can be seen from Table 1, the specific surface areas pass through a maximum for the X-ray amorphous phases (e.g., 50% Cr) and fall to a minimum of 5 m^2/g for the chromium hydroxyfluoride (100% Cr).

More or less the same effect was observed for the catalytic activity (Fig. 2). Due to the selected experimental conditions a clear gradation between the highly active samples (3, 10, 50% Cr) was not possible with this technique.

Considering the activation of the samples one can state that the undoped β-AlF_3 is not immediately active. Previous studies with $CHClF_2$ (instead of CCl_2F_2) (4, 5) have shown that traces of moisture have a significant influence on that initial activation period due to the blockage of Lewis acid sites. Since CCl_2F_2 is more stable, it takes more time to remove the surface water.

The ammonia temperature-programmed desorption enables a further gradation among the samples (Table 1). Here, the amount of desorbed ammonia is given for a desorption temperature interval 325–400°C indicating a certain strength of acid sites. As we know from detailed studies (5), this temperature range represents an acid strength that is required for the catalysis of the dismutation reaction. The highly active 50, 10, and 3% Cr samples exhibit higher amounts of ammonia desorption (more strong sites) compared to the less active 80% Cr sample. The chromium hydroxyfluoride exhibits the lowest desorption intensity in that area. Therefore, it is not surprising that the chromium hydroxyfluoride is catalytically inactive (see Fig. 2).

The nature of the acid sites can be determined with the characteristic infrared bands arising from pyridine chemisorbed on the solid surface (5) and references therein). With exception of the 50% Cr sample, where a very slight Brønsted acidity has been detected besides a large excess of Lewis acidity, all the other samples exhibit only Lewis acid sites. Figure 3 shows the intensities of the 19*b* ring mode vibration of chemisorbed pyridine at 1453 cm^{-1}, indicating Lewis acid sites. The bands at approximately 1493 cm^{-1} can be assigned to the 19*a* vibration (Lewis acid sites), but they are less intense. As can be seen from the band intensities at 1453 cm^{-1}, the number of Lewis acid sites grows with increasing Cr content, passes through a maximum at 50% Cr, and then falls. On the other hand, an alteration of the strength of the Lewis sites is not observed. This can be concluded from the absence of a significant wavenumber shift. At the chromium hydroxyfluoride (100% Cr) the 19*b* pyridine band is no longer detectable. The general tendency in the amounts of Lewis acid sites is comparable with the observed behavior in BET surface areas, ammonia desorption intensities (strong acid sites), and catalytic activity. Independent of that, there is an apparent discrepancy between the ammonia desorption for chromium hydroxyfluoride (101 μmol/g, Table 1) and the absence of the pyridine band (Fig. 3). It can be rationalized

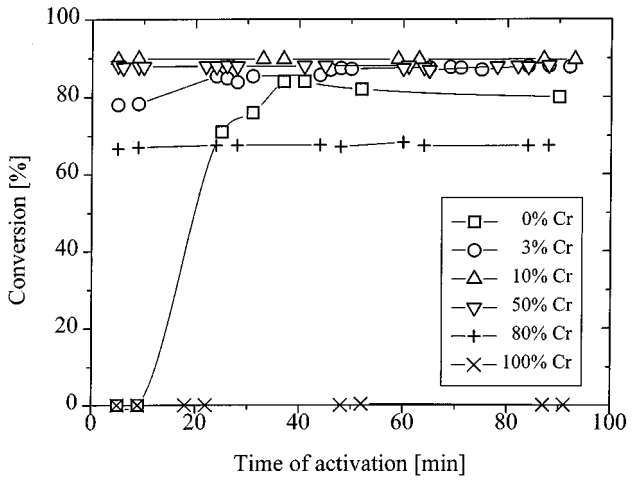

FIG. 2. Conversion of CCl_2F_2 versus activation time for various Cr-replaced α-$AlF_3 \cdot 3H_2O$ calcination products (catalyst weight = 600 mg, residence time = 2 s, 390°C).

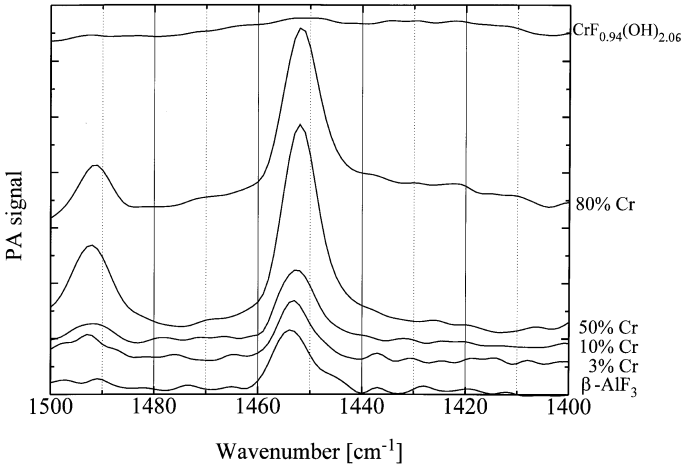

FIG. 3. FTIR photoacoustic spectra (offset) of pyridine chemisorbed on Cr-replaced α-$AlF_3 \cdot 3H_2O$ calcination products (background correction, 80 mg catalyst weight, 30μl pyridine adsorption at 150°C, flow system).

by the different diameter of the particular probe molecule. The small ammonia molecule can reach the acid sites, but the larger pyridine molecule cannot do so.

β-CrF₃

Since the calcination of α-$CrF_3 \cdot 3H_2O$ did not result in the formation of HTB-β-CrF_3, alternative routes for its synthesis were applied. In a first approach the calcination was carried out under vacuum at various calcination temperatures. In all cases X-ray amorphous phases were obtained. Therefore, we have changed to another method. HTB-β-CrF_3 can be produced by thermal decomposition of $(NH_4)_3CrF_6$using quasi-isobaric conditions (24). Here, the starting substance is free of water, but the calcined sample is expected to contain traces of unliberated ammonium. Hence, it is not entirely justified to compare the properties of the particular product samples. However, a qualitative interpretation seems to be possible. The catalytic activity of β-CrF_3 is comparable with those of the highly active 3, 10, or 50% Cr samples, although the BET surface area is rather low (36 m^2/g). The FTIR photoacoustic spectrum of pyridine chemisorbed on β-CrF_3 reveals small bands at 1453 and 1618 cm^{-1} indicating Lewis acid sites. Unfortunately, the sample contains traces of ammonium and its vibrations appear in the same region of the IR spectrum. Even calcination procedures under vacuum could not entirely prevent the presence of ammonium.

Replacement by Magnesium

In the Mg series precipitates of α-$AlF_3 \cdot 3H_2O$ and MgF_2 were obtained. In the case of the 50% Mg sample traces of aluminum hydroxyfluoride were also formed. Consequently, the calcined sample contains traces of X-ray amorphous oxides (Table 2).

Figure 4 presents the XRD patterns of the calcined samples indicating a loss of crystallinity for β-AlF_3 with increasing Mg content. Obviously, the dopant disturbs the crystallization of the main phase. With further increase of the Mg content, the reflections of MgF_2 become more and more visible.

Very slight increases of the β-AlF_3 lattice constants, particularly at the 50% sample, were detected. Furthermore, the pattern of the reflection intensities differs from the other samples. A partial insertion of Mg into the β-AlF_3 lattice is assumed.

The specific surface area is rising steadily with increasing Mg content (Table 2). The catalytic activity slightly improves up to 10% Mg, but falls to zero at higher Mg concentrations (see Fig. 5). The conversion is therefore not proportional to the BET surface area.

The amounts of ammonia TPD are shown in Table 2. The relevant region between 325 and 400°C reflects the gradation of catalytic activity. The inactive 50% Mg and MgF_2 samples exhibit the lowest amounts of ammonia desorption

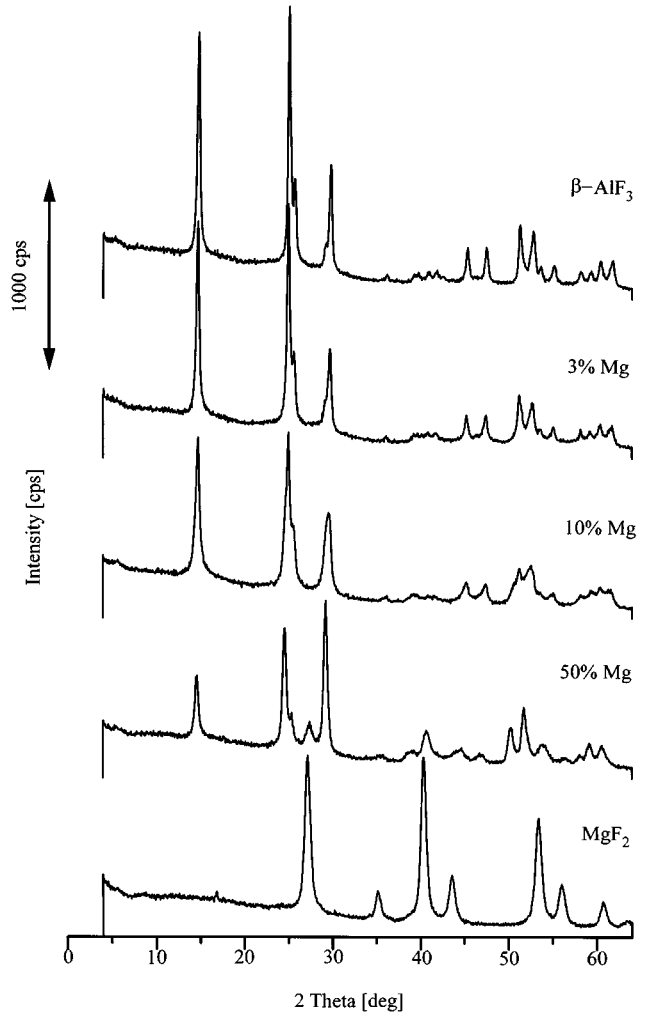

FIG. 4. XRD patterns (offset) of α-$AlF_3 \cdot 3H_2O$ calcination products with stepwise replacement by Mg. Note the coexistence of both β-AlF_3 and MgF_2 at the 50% Mg sample.

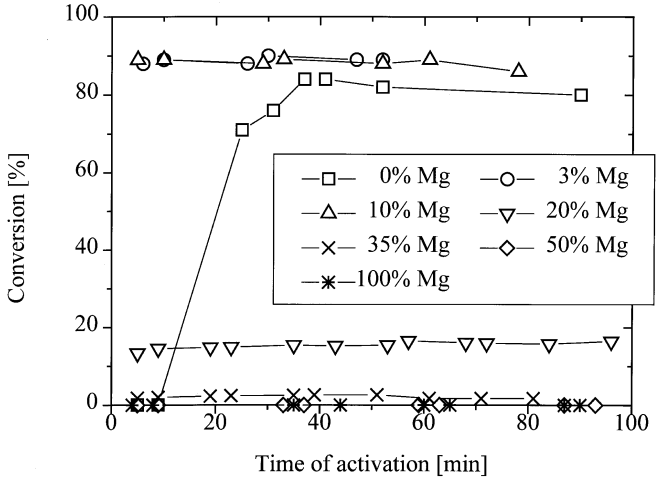

FIG. 5. Conversion of CCl_2F_2 versus activation time for various Mg-replaced α-$AlF_3 \cdot 3H_2O$ calcination products (catalyst weight = 600 mg, residence time = 2 s, 390°C).

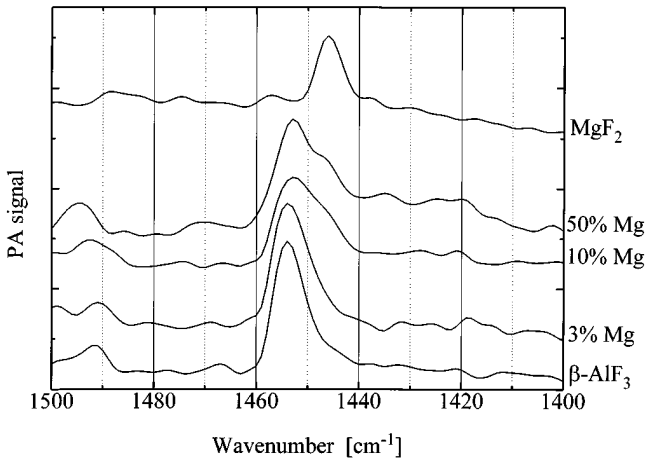

FIG. 6. FTIR photoacoustic spectra (offset) of pyridine chemisorbed on Mg-replaced α-$AlF_3 \cdot 3H_2O$ calcination products (background correction, 80 mg catalyst weight, 30μl pyridine adsorption at 150°C, flow system).

in that region, although their surface areas exceed those of the others.

The coexistence of two lattices in the 50% Mg sample is accompanied by a coexistence of two types of different Lewis acid sites. As can be seen from Fig. 6, the 50% Mg sample has a shoulder just at the wavenumber which corresponds with the MgF_2 Lewis sites (1446 cm^{-1}). The strength of these sites is not sufficient to catalyze the dismutation. MgF_2 and pure γ-alumina (19*b* band at 1447 cm^{-1} (5) are catalytically inactive.

DISCUSSION

The calcination of α-$AlF_3 \cdot H_2O$ under the appropriate conditions led to the formation of pseudo-hexagonal tungsten bronze (HTB)-β-AlF_3, whereas the isotypic α-$CrF_3 \cdot H_2O$ formed the cubic pyrochlore phase $CrF_{3-x}(OH)_x$. In the latter compound a partial hydrolysis has occurred. The higher acidity of chromium cations enables a polarization of the water molecule. HF is liberated and Cr–OH bonds are formed. This phenomenon is also well established in surface chemistry. Kania and Jurczyk (9) reported that due to the higher electronegativity of Cr^{3+} an even higher extent of dissociative chemisorption of water was observed. As a result, the Cr-doped Al_2O_3 offered a higher Brønsted acidity than pure Al_2O_3. The formation of pyrochlore chromium hydroxyfluoride is accompanied by a dramatic loss of catalytic activity that is independent from the decrease of BET surface area. Catalytic inactivity is also known for the isotypic aluminum hydroxyfluoride compound (4). From our results it can be concluded that Lewis acid sites on the surface of the pyrochlore structure are less attainable compared with HTB-β-AlF_3 or β-CrF_3 surfaces. This is not restricted to the Lewis acid sites, since the BET surface areas also reveal considerable differences between both structures (β-AlF_3: 31 m^2/g, β-CrF_3: 36 m^2/g, but $CrF_{0.94}(OH)_{2.06}$: 5 m^2/g). How can this be explained? In a first approach we have compared their crystal structures. Figure 7 illustrates the specific octahedra linking in the HTB structure (a) and the pyrochlore structure (b). The general formula of the pyrochlore can be written as $A_2B_2X_6X'$. *B* represents chromium and *X* is fluoride or hydroxide. The *A* and *X*' positions are not occupied in chromium hydroxyfluoride. Both the HTB and the pyrochlore structure contain hexagonal channels (see Figs. 7), their diameter in the HTB phase being about 350 pm. Nitrogen and water should be able to enter these channels, but C_1 halocarbon can only deposit tetrahedra on the entry of the channel.

The distribution of channels within the unit cells is different. In the HTB structure the channels are directed

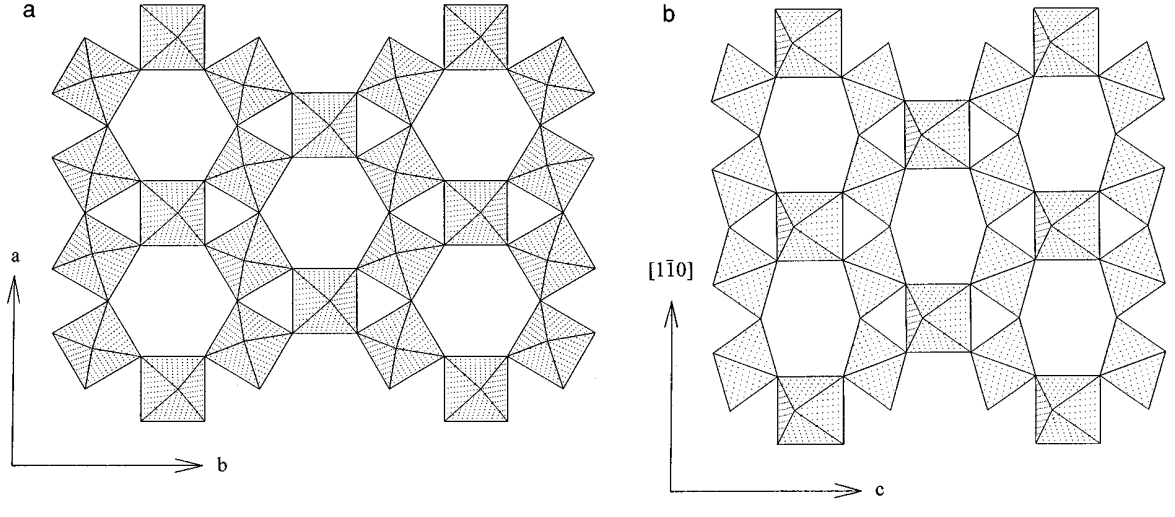

FIG. 7. Linking of MX_6 octahedra (a) in the HTB structure of β-AlF_3 in the [001] direction and (b) in the pyrochlore structure of $CrF_{0.94}(OH)_{2.06}$ in the [110] direction (one of six channel directions).

along the *c* axis (only one direction, no cross), whereas the channels in the pyrochlore structure pass along all six plane diagonals of the cubic unit cell. Their cross angles are 90° and 60°, respectively. As can be concluded, the crystal density of the pyrochlore structure is much lower than in the HTB structure. It is therefore somewhat surprising that the accessibility for nitrogen molecules (BET) in the pyrochlore sample is lower than in the HTB sample. This indicates that the inner surface of the pyrochlore chromium hydroxyfluoride is not attainable. This could be effected by hydroxyl groups which form hydrogen bridge bonds (confirmed by infrared spectroscopy). It can be assumed that the crystal surfaces of the hydroxyfluoride are reconstructed. This results in a decrease of adsorptive capacity, e.g., low BET surface area. In the case of the HTB trifluorides β-AlF_3 (or β-CrF_3) an improved accessibility is expected.

A further reason for the catalytic activity of the HTB β-AlF_3 (or β-CrF_3) could be derived from the different crystallographic cleavabilities of the HTB and pyrochlore structures. The HTB lattice has well-defined cleavage planes since its channels pass in one direction only. It is often observed in catalysis that the presence of well-defined crystal surfaces promotes the catalytic activity. On the other hand, the pyrochlore structure does not have a favored cleavage surface, as is known for pyrochlore minerals (25).

Moreover, the inductive effect of fluoride also has an influence on the strength of the Lewis acid sites and catalytic activity. Metal cations surrounded by fluoride ligands exhibit a higher Lewis acid strength than oxides or hydroxides (5, 26). Hydroxyfluorides are therefore expected to show a lower Lewis strength than fluorides.

Let us consider now the samples with Cr contents up to 80%, their catalytic activity as well as ammonia TPD (region of acid sites between 325 and 400°C) and the intensities of the 19*b* ring mode vibration of pyridine chemisorbed on Lewis acid sites. All these surface properties follow the course of the specific surface areas of the samples. From the absence of a significant wavenumber shift in the 19*b* pyridine ring mode vibration (see Fig. 3), it can be concluded that the Lewis strength remains unchanged, whereas the number of sites increases with higher Cr contents. The steady loss of crystallinity, accompanied by an increase of BET surface area, improves the accessibility of the Lewis acid sites (metal cations). Hence, larger amounts of ammonia and pyridine can be adsorbed and the conversion of dismutation is enhanced. Since the 50 and 80% Cr samples were X-ray amorphous it is not clear what kind of short-range order these samples possess. For this reason XPS was applied (27) to clarify whether the samples are homogeneous or consist of several components. We were able to conclude from the shape of the F1*s*, Cr 2*p*, and Al 2*s* spectra that the samples consist of homogeneous metal fluoride species with increasing OH for F substitution with growing Cr content. Further investigations including an EXAFS study will be published in due course.

If the Cr content exceeds about 90% the new pyrochlore phase with different surface properties becomes more and more dominating. Although the obtained crystallinity is quite low one can state that the surface as well as the catalytic properties are comparable with the chromium hydroxyfluoride of improved crystallinity that was synthesized solvothermally (28).

Considering the Mg doped samples the following behavior is observed. There are two contrary processes. The insertion of magnesium cations disturbs the lattice, enlarges the BET surface area, and improves the accessibility of the Lewis sites (conversion increases). On the other hand, the increasing Mg content leads to a decrease of the Lewis acid strength (wavenumber shift downward, Fig. 6). Therefore, the conversion has a maximum (10% Mg). The difference compared to the replacement by Cr is the disagreement between BET surface area and catalytic reactivity. Obviously, MgF_2 possesses a sufficient amount of sites, but their strength is too weak. Concerning the 50% Mg sample, it is not entirely clear why the presence of strong Lewis sites (besides weak sites) does not lead to catalytic activity for this sample. It cannot be excluded that the coexistence of two different types of Lewis sites has an influence on the catalytic mechanism. Possibly, they do not act independently. On the other hand, the geometrical conditions on the 50% Mg sample differ from those of the previous samples, since XRD revealed a slight increase of the HTB lattice constants. The partial insertion of Mg into β-AlF_3 led to a slight opening of the lattice. Possibly, this has a negative influence on the catalysis.

The final question that should be discussed is whether there is any possibility of prediction for the acid strength and catalytic activity of doped compounds. Here, the following problems should be noted. One important factor is the partial charge of the particular cation that can be calculated with the help of Sanderson's electronegativity values (29). These partial charges themselves significantly depend on the particular anion. Even if the same anion is considered there are still discrepancies if one compares the calculated partial charge of the cation with the experimental Lewis acid strength. The reason is that the accessibility of the given cation must be taken into consideration. The higher the partial charge of the cation the smaller its ionic diameter and the larger the ionic diameter of the particular anion. The accessibility of the cations can decrease with increasing partial charge. Therefore, the experimental Lewis acid strength is mainly influenced by the geometric conditions within a given lattice and its particular surface structure. Work is currently in progress to collect more data and to develop a model for acid sites on metal fluoride surfaces.

ACKNOWLEDGMENTS

We are grateful to Fonds der Chemischen Industrie and Deutsche Forschungsgemenischaft for financial support.

REFERENCES

1. Manzer, L. E., Eur. Patent 331991, to E.I.Du Pont de Nemours and Co., 1989.
2. Hirayama, S., PCT Int. App., WO 8910341, to Showa Denko K. K., 1989.
3. Manzer, L. E., U.S. Patent 4766259, to E. I. Du Pont de Nemours and Co., 1988.
4. Hess, A., Kemnitz, E., Lippitz, A., Unger, W. E. S., and Menz, D. H., *J. Catal.* **148**, 270 (1994).
5. Hess, A., Kemnitz, E., and *J. Catal.* **149**, 449 (1994).
6. Berteau, P., and Delmon, B., *Catal. Today* **57**, 121 (1989).
7. Berteau, P., Kellens, M. A., and Delmon, B., *J. Chem. Soc., Faraday Trans.* **87**, 1425 (1991).
8. Schurch, J., Cant, N. W., and Trimm, D. L., *Appl. Catal.* **101**, 105 (1993).
9. Kania, W., and Jurczyk, K., *Appl. Catal.* **61**, 27 (1990).
10. Hamada, H., Kinataichi, Y., Sasaki, M., and Ito, T., *Appl. Catal.* **75**, L1 (1991).
11. Morterra, C., Magnacca, H., Cerrato, L., del Favero, G., Fillipi, K., and Folonari, G., *J. Chem. Soc., Faraday Trans.* **88**, 135 (1992).
12. Wendt, G., Meinicke, C. D., and Schmitz, W., *Appl. Catal.* **45**, 209 (1988).
13. Kania, W., and Jurczyk, K., *Appl. Catal.* **56**, 253 (1989).
14. DeCanio, E. C., Bruno, J. W., Nero, V. P., and Edwards, J. C., *J. Catal.* **140**, 84 (1993).
15. Bechadergue, D., Blanchard, M., and Canesson, P., *Appl. Catal.* **20**, 179 (1986).
16. Wells, A. F., "Structural Inorganic Chemistry." Clarendon, Oxford, 1993.
17. Fresenius, W., and Jander, S., "Handbuch der analytischen Chemie," Springer-Verlag, Berlin, 1959.
18. Kemnitz, E., Hass, D., and Grimm, B., *Z. Anorg. Allg. Chem.* **589**, 228 (1990).
19. Kemnitz, E., Hansen, G., Hess, A., and Kohne, A., *J. Mol. Catal.* **77**, 193 (1992).
20. Le Bail, A., Jacobini, C., LeBlanc, M., dePape, R., Duroy, H., and Fourquet, J. L., *J. Solid State Chem.* **77**, 96 (1988).
21. Rault, M., Demazeau, G., Portier, J., and Grannec, J., *Bull. Soc. Chim. Fr.* **1**, 74 (1970).
22. Fourquet, J. L., Riviere, M., LeBail, A., Nygrens, M., and Grins, J., *Eur. J. Solid State Inorg. Chem.* **25**, 535 (1988).
23. Menz, D. H., Mensing, C., Hönle, W., von Schnering, H. G., *Z. Anorg. Allg. Chem.* 611, 107 (1992).
24. Menz, D. H., and Bentrup, U., *Z. Anorg. Allg. Chem.* **613**, 108 (1992).
25. Rösler, H. J., "Lehrbuch der Mineralogie." p. 392. Deutscher Verlag für Grundstoffindustrie, Leipzig, 1984.
26. Peri, J. B., *J. Phys. Chem.* **72**, 2917 (1968).
27. Grohmann, I., Hess, A., and Kemnitz, E., unpublished work.
28. Adamczyk, B., Diplomarbeit, Humboldt-Universität, Berlin, 1995.
29. West, A. R., "Grundlagen der Festkörperchemie." VCH, Weinheim, 1992.